

# Uncertainty Analysis for Curved Surface Contact Patches

Dimitrios Kanoulas, Nikos G. Tsagarakis, and Marsette Vona

**Abstract**—We present a Gaussian uncertainty analysis of bounded curved patches that fit to local rough surfaces and are suitable for representing foothold or handhold contacts between an articulated robot and the environment. The input is a set of 3D point samples with  $3 \times 3$  covariance matrices that express their Gaussian uncertainty. We first introduce uncertainty propagation of geometrical patch parameters during fitting on range samples. The output for each patch includes a covariance matrix in its parametric space. We also introduce a set of distance metrics to validate the magnitude of the propagated uncertainty and we run a set of tests on various range data. The importance of this paper lies in the uncertainty analysis for curved contact patches that can be further applied during locomotion or manipulation.

## I. INTRODUCTION

Robots with limbs often require reliable contact with the environment. Exteroceptive sensing, such as range measurement, plays an important role in detecting contact areas from a distance and planning for foothold or handhold placement. The problem becomes particularly interesting with irregular surfaces, where the uncertainty of the environment is significant and the input data are subject to sensing errors. To reason about any contact with a surface using range data, an uncertainty analysis can help evaluate the risk of the action.

In prior work [1] we introduced a set of bounded curved patches (Fig. 1) to model contacts on rough terrain using geometrically meaningful parameters. We also presented an algorithm to fit patches to noisy heteroskedastic (non-uniform variance) point cloud data from a range sensor. In this paper, we first present the detailed error propagation during the patch fitting process, assuming Gaussian uncertainty in the input range data, expressed as a  $3 \times 3$  covariance matrix (ellipsoid in the 3D Euclidean space). The fitted patch's uncertainty is also expressed as a covariance matrix in its parametric space. We then describe a set of quantitative distance metrics to evaluate the magnitude of the propagated uncertainty based on the covariance. The advantage of patch parametrization is that it is geometrically meaningful, expressing poses (i.e., rotations and translations), curvatures, and lengths/angles for the boundaries. Thus, the uncertainty propagation has a direct geometric meaning that can be analyzed and used for risk evaluation during a contact planning.

Dimitrios Kanoulas and Nikos G. Tsagarakis are with the Department of Advanced Robotics, Istituto Italiano di Tecnologia (IIT), Via Morego 30, 16163, Genova, Italy. {Dimitrios.Kanoulas, Nikos.Tsagarakis}@iit.it

Marsette Vona was with the College of Computer and Information Science, Northeastern University, Boston, Massachusetts, at the time of the associated work. vona@jpl.nasa.gov

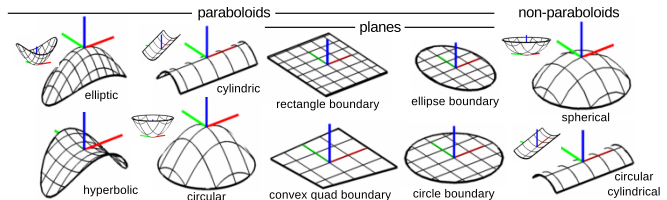


Fig. 1. Patch types and local coordinate frames, introduced in [1].

This work is the first to discuss uncertainty evaluation for curved contact patches with geometrically meaningful parameters using range data. We consider this task necessary and important for handhold or foothold contact planning with irregular surfaces. Moreover, the patches with their uncertainty could potentially serve as features for feature-based 3D mapping in the context of SLAM (Simultaneous Localization and Mapping), in a similar way that has been used in [2] for planes, providing a faster and more space efficient representation. We experimentally evaluate the uncertainty propagation on point cloud samples both from simulated and real range sensors. We have implemented the proposed approach in the Surface Patch Library (SPL), with sourcecode available on our website [3].

Next we cover related work, followed by a review of the patch modeling and fitting process along with the uncertainty propagation on heteroskedastic range data. Then we describe the evaluation distance metrics for the Gaussian uncertainty in the patch parametric space. Finally, we experimentally validate the error propagation on simulated and real range samples.

### A. Related Work

Modeling surfaces using range data either for contact [4], [5] or mapping [2] has a significant history in robot locomotion [6] and manipulation [7]. The importance of representing uncertainty goes back to the origins of robotics [8], especially for 3D range data [9], but only recently has been considered for mobile manipulators [10] and rough terrain robots [11].

Most of the work in the past has been focused on modeling range data uncertainty so that it can be used during a typical Kalman-type SLAM system. Gaussian modeling with covariance matrices is one of the ways to quantify uncertainty and we will use this representation in this paper. There has been a lot of work on how to determine the covariance matrices for range data. We are going to use the approach introduced in [12], which is based on a pointing/disparity stereo error model. Recently, an uncertainty model for the Kinect sensor has been introduced in [13], while a mixture of Gaussians has been also used in [14], providing alternative construction methods of covariance matrices.

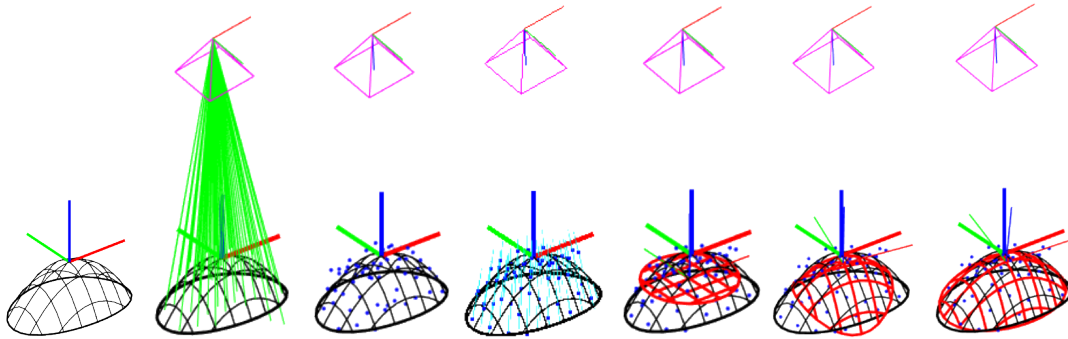


Fig. 2. A paraboloid patch fitting: (i) the original paraboloid patch, (ii) the frustum and the measurement rays, (iii) 60 noisy sample range data, (iv) error ellipsoids, (v) plane fitting, (vi) unbounded patch fitting, and (vii) boundary fitting.

Depending on the robotic application, Gaussian uncertainties on range data have been propagated to various high level structures that were used for contacts between robots and the environment. For instance, [15] propagates them to elevation maps, while [4], [5] to planar surfaces. The latter work is the closest approach that this paper compares to, with the difference that we provide propagation to bounded curved surfaces that are geometrically parametrized, while considering heterodastic range data uncertainties during the fitting and error propagation. These type of uncertainties are going to affect the way that a robot may contact a surface.

## II. PATCH MODELING AND FITTING

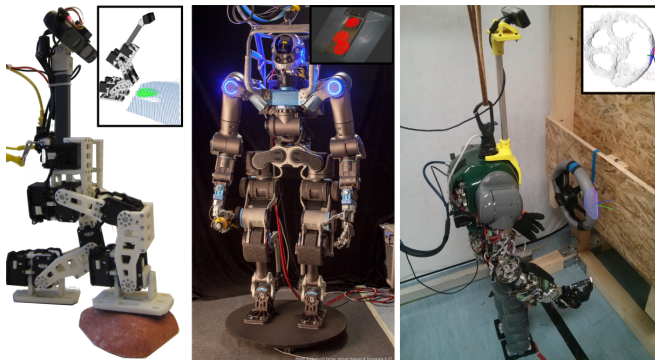


Fig. 3. The RBPB [16], WALK-MAN [17], and COMAN [18] robots use the bounded curved patches framework for locomotion and manipulation.

To model irregular surfaces of the size of the contacts between a robot hand/foot and the environment, we introduced in [1] a set of ten bounded curved patches—eight paraboloids and two non-paraboloids (Fig. 1)—that balance expressiveness with compactness of representation. These patches have been later used for locomotion [16], [17] and manipulation [18] on three different humanoid robots (Fig. 3). We briefly review elliptic/hyperbolic paraboloid’s geometric parametrization, while in the next section we present the uncertainty propagation based on all patch types. We also describe in brief the patch fitting process using point cloud data that come from a range sensor with their uncertainty expressed as  $3 \times 3$  covariance matrices. Due to space constraints we must refer readers to the original paper for a full model and a detailed algorithm description.

Patches have two types of intrinsic parameters depending on their model (up to two principal curvatures  $\kappa_{x,y}$  and up

to five boundary lengths and angles) and up to six extrinsic parameters ( $\mathbf{r} \in \mathbb{R}^3$  rotation and  $\mathbf{c} \in \mathbb{R}^3$  translation vector) that provide the pose of the local coordinate frame of each patch in the world frame (Table I). For instance, the implicit form for a paraboloid patch in its local frame is:

$$\mathbf{q}_i^T \text{diag}(\kappa_x, \kappa_y, 0) \mathbf{q}_i - 2\mathbf{q}_i^T [0 \ 0 \ 1]^T = 0, \quad (1)$$

where  $\mathbf{q}_i \in \mathbb{R}^3$  is a point on the patch. Elliptic/hyperbolic paraboloid patches are bounded with ellipses in the local  $xy$  patch frame axes, which are aligned and centered at  $\mathbf{c}$ . We parametrize an ellipse with its radii  $\mathbf{d}_e \triangleq [d_x \ d_y]^T$  as a subset of the full surface that satisfies:

$$0 \geq \mathbf{u}^T \text{diag}([1/d_x^2 \ 1/d_y^2]) \mathbf{u} - 1, \quad (2)$$

where  $\mathbf{u}$  is the projection of all 3D points  $\mathbf{q}_i$  on the local  $xy$  patch frame.

The fitting process takes as input  $N$  3D points  $\mathbf{q}_i \in \mathbb{R}^3$ , their covariance matrices  $\Sigma_i \in \mathbb{R}^{3 \times 3}$ , a patch type  $s \in \{\text{parab, plane, sphere, ccyl}\}$ , and a boundary type  $b \in \{\text{ellipse, circle, aarect, cquad}\}$  if the patch type is a  $s = \text{plane}$  (otherwise it is implied). The output is the patch parameters that were described above. In this paper we extend the method to also include the uncertainty of the patch as a covariance matrix  $\Sigma \in \mathbb{R}^{p \times p}$ , where  $p$  is the DoF of the patch type. The fitting proceeds in two stages, where first an unbounded surface is fitted followed by the bound fitting, using the projected to the local  $xy$  plane sample points. An important aspect of the process that was described in [1] has to do with the nonlinear  $\chi^2$  fitting problem and the optimization solution that we proposed—named weighted Levenberg-Marquardt (WLM)—where the heterodastic variance of the sample points are considered during the fitting. The WLM method returns by design the covariance matrix  $\Sigma \in \mathbb{R}^{p \times p}$  of the fitted surface. In the next section we will go through the fitting algorithm as described in [1] and mathematically formulate the first order error propagation.

## III. GAUSSIAN UNCERTAINTY PROPAGATION

We now present the first order error propagation [19] for the Gaussian uncertainty model expressed as a covariance matrix  $\Sigma \in \mathbb{R}^{p \times p}$  in the patch parametric space  $p$ . The input covariance matrix  $\Sigma_i \in \mathbb{R}^{3 \times 3}$  for each input sample point  $\mathbf{q}_i \in \mathbb{R}^3$  has been determined experimentally following

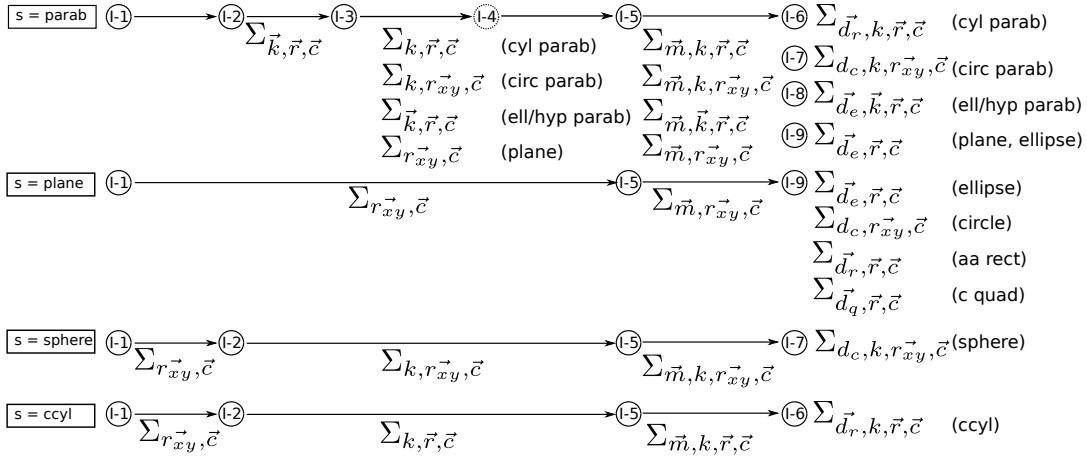


Fig. 4. Uncertainty propagation diagram.

the process that was described in [12] for the Kinect sensor. The pointing stereo error was estimated as  $\sigma_{\text{point}} = 0.35\text{px}$ , while the disparity stereo error as  $\sigma_{\text{disp}} = 0.17\text{px}$ . A similar experimental analysis can be performed for any other range sensor that may be available on a robotic platform. In each step the input patch covariance matrix  $\Sigma$  will either come from the WLM fitting algorithm or from the previous propagation step.  $\Sigma$ 's subscripts are the parameters that are included each time in the covariance matrix in the particular order that they are referenced. A diagram of the propagation is visualized in Fig. 4, while a paraboloid patch fitting is illustrated in Fig. 2. We skip all the tedious but trivial partial derivative computations, while the detailed reasoning behind each fitting step and the pose representation choices can be reviewed in [1].

### Stage I-1 Plane Fitting

(i) First a Linear Least-Squares plane fitting takes place for the input point samples  $q_i$ , ignoring their uncertainty  $\Sigma_i$ . If  $s \neq \text{parab}$ , the plane is re-fitted using the WLM method. The *output* will be the rotation vector  $\mathbf{r}_{xy} \in \mathbb{R}^2$  (considering the symmetry around the local z-axis), the translation vector  $\mathbf{c} \in \mathbb{R}^3$ , and the covariance matrix of the  $[\mathbf{r}_{xy} \ \mathbf{c}]$  vector  $\Sigma_{\mathbf{r}_{xy}, \mathbf{c}} \in \mathbb{R}^{5 \times 5}$ , coming from the WLM fitting.

(ii) We then set  $\mathbf{c}' = \bar{\mathbf{q}} - \hat{z}_\ell^T (\bar{\mathbf{q}} - \mathbf{c}) \hat{z}_\ell$ , where  $\bar{\mathbf{q}} = (\sum_{i=1}^N \mathbf{q}_i) / N$ ,  $\hat{z}_\ell = \mathbf{R}(\mathbf{r}) \hat{z}$ , and  $\mathbf{r} = [\mathbf{r}_{xy} \ 0]$ . Since in this step we only change the position vector  $\mathbf{c}$  after the WLM fitting, the propagated *output* covariance  $\Sigma_{\mathbf{r}_{xy}, \mathbf{c}'}$   $\in \mathbb{R}^{5 \times 5}$  will be:

$$\Sigma_{\mathbf{r}_{xy}, \mathbf{c}'} = \mathbf{J} \Sigma \mathbf{J}^T \quad (3)$$

$$\mathbf{J} = \begin{bmatrix} \mathbf{0}_{2 \times 3} & \mathbf{0}_{2 \times 3} & \mathbf{I}_{2 \times 2} & \mathbf{0}_{2 \times 3} \\ \frac{\partial \mathbf{c}'^T}{\partial \hat{z}_\ell} & \frac{\partial \mathbf{c}'^T}{\partial \bar{\mathbf{q}}} & \frac{\partial \mathbf{c}'^T}{\partial \mathbf{r}_{xy}} & \frac{\partial \mathbf{c}'^T}{\partial \mathbf{c}} \end{bmatrix} \in \mathbb{R}^{5 \times 11}$$

$$\Sigma = \begin{bmatrix} \Sigma_{\hat{z}_\ell} & \mathbf{0}_{3 \times 3} & \mathbf{0}_{3 \times 3} \\ \mathbf{0}_{3 \times 3} & \Sigma_{\bar{\mathbf{q}}} & \mathbf{0}_{3 \times 3} \\ \mathbf{0}_{5 \times 5} & \mathbf{0}_{5 \times 5} & \Sigma_{\mathbf{r}_{xy}, \mathbf{c}} \end{bmatrix} \in \mathbb{R}^{11 \times 11}$$

$$\Sigma_{\hat{z}_\ell} = \left( \frac{\partial \mathbf{R}}{\partial \mathbf{r}} \hat{z} \right) \Sigma_{\mathbf{r}} \left( \frac{\partial \mathbf{R}}{\partial \mathbf{r}} \hat{z} \right)^T, \Sigma_{\bar{\mathbf{q}}} = \frac{1}{N^2} \sum_{i=1}^N \Sigma_i$$

### Stage I-2 Unbounded Surface Fitting

(i) If  $s \neq \text{plane}$ , an unbounded patch surface is fitted using

WLM, with the initial parameters from the previous step.

If  $s = \text{parab}$ , the WLM output is the curvature vector  $\mathbf{k} = [\kappa_x \ \kappa_y] \in \mathbb{R}^2$ , the rotation vector  $\mathbf{r} \in \mathbb{R}^3$ , the translation vector  $\mathbf{c} \in \mathbb{R}^3$ , and the covariance matrix of the  $[\mathbf{k} \ \mathbf{r} \ \mathbf{c}]$  vector  $\Sigma_{\mathbf{k}, \mathbf{r}, \mathbf{c}} \in \mathbb{R}^{8 \times 8}$ . If the side-wall effect is handle by reparametrization (see [3]), then a single patch parameter  $c \in \mathbb{R}$  is replacing the  $\mathbf{c}$  and thus  $\Sigma_{\mathbf{k}, \mathbf{r}, \mathbf{c}} \leftarrow \mathbf{J} \Sigma \mathbf{J}^T \in \mathbb{R}^{6 \times 6}$ , where  $\mathbf{J} = \mathbf{I}_{6 \times 8}$ , with  $\mathbf{J}(6 : 8, 6) = \hat{z}_\ell$  (i.e. the plane normal vector from previous step).

If  $s = \{\text{ccyl}, \text{sphere}\}$ , the WLM *output* is a curvature  $k \in \mathbb{R}$ , the rotation matrix  $\mathbf{r}_{xy}$ , the translation vector  $\mathbf{c} \in \mathbb{R}^3$ , and the covariance matrix  $\Sigma_{k, \mathbf{r}_{xy}, \mathbf{c}} \in \mathbb{R}^{6 \times 6}$ .

(ii) If  $s = \text{sphere}$ ,  $\mathbf{r}_{xy}$  is replaced with the one of Stage I-1 ( $\mathbf{r}'_{xy} \leftarrow \mathbf{r}_{xy}$ ) and thus:

$$\Sigma_{k, \mathbf{r}'_{xy}, \mathbf{c}} = \mathbf{J} \Sigma_{k, \mathbf{r}_{xy}, \mathbf{c}} \mathbf{J}^T \in \mathbb{R}^{6 \times 6} \quad (4)$$

$$\mathbf{J} = \begin{bmatrix} \mathbf{0}_{1 \times 2} & 1 & \mathbf{0}_{1 \times 3} \\ \mathbf{I}_{2 \times 2} & \mathbf{0}_{2 \times 1} & \mathbf{0}_{2 \times 3} \\ \mathbf{0}_{3 \times 2} & \mathbf{0}_{3 \times 1} & \mathbf{I}_{3 \times 3} \end{bmatrix} \in \mathbb{R}^{6 \times 6}$$

If  $s = \text{ccyl}$ , we set  $\mathbf{r}' = \mathbf{r}(\mathbf{R}_\ell) = \mathbf{r}([\hat{x}_\ell \ \hat{y}_\ell \ \hat{z}_\ell])$  (log map),  $\hat{z}_\ell = \mathbf{R}(\mathbf{r}) \hat{z}$ ,  $\hat{x}_\ell = \mathbf{R}(\mathbf{r}) \hat{x}$ , and  $\hat{y}_\ell = \hat{z}_\ell \times \hat{x}_\ell = [\hat{x}_\ell]_\times^T \hat{z}_\ell = [\hat{z}_\ell]_\times \hat{x}_\ell$ . Thus, the covariance matrix  $\Sigma_{k, \mathbf{r}', \mathbf{c}} \in \mathbb{R}^{7 \times 7}$  can be calculated as follows:

$$\Sigma_{k, \mathbf{r}', \mathbf{c}} = \mathbf{J} \Sigma_{\hat{z}_\ell, \hat{x}_\ell, k, \mathbf{c}} \mathbf{J}^T \in \mathbb{R}^{7 \times 7} \quad (5)$$

$$\mathbf{J} = \begin{bmatrix} \mathbf{0}_{1 \times 3} & \mathbf{0}_{1 \times 3} & 1 & \mathbf{0}_{1 \times 3} \\ \frac{\partial \mathbf{r}'}{\partial \hat{z}_\ell} & \frac{\partial \mathbf{r}'}{\partial \hat{x}_\ell} & \mathbf{0}_{3 \times 1} & \mathbf{0}_{3 \times 3} \\ \mathbf{0}_{3 \times 3} & \mathbf{0}_{3 \times 3} & \mathbf{0}_{3 \times 1} & \mathbf{I}_{3 \times 3} \end{bmatrix} \in \mathbb{R}^{7 \times 10}$$

$$\Sigma_{\hat{z}_\ell, \hat{x}_\ell, k, \mathbf{c}} = \begin{bmatrix} \Sigma_{\hat{z}_\ell} & \mathbf{0}_{3 \times 3} & \mathbf{0}_{3 \times 4} \\ \mathbf{0}_{3 \times 3} & \Sigma_{\hat{x}_\ell} & \mathbf{0}_{3 \times 4} \\ \mathbf{0}_{4 \times 3} & \mathbf{0}_{4 \times 3} & \Sigma_{k, \mathbf{c}} \end{bmatrix} \in \mathbb{R}^{10 \times 10}$$

$$\Sigma_{\hat{z}_\ell} = \left( \frac{\partial \mathbf{R}}{\partial \mathbf{r}} \hat{z} \right) \Sigma_{\mathbf{r}} \left( \frac{\partial \mathbf{R}}{\partial \mathbf{r}} \hat{z} \right)^T, \Sigma_{\hat{x}_\ell} = \left( \frac{\partial \mathbf{R}}{\partial \mathbf{r}} \hat{x} \right) \Sigma_{\mathbf{r}} \left( \frac{\partial \mathbf{R}}{\partial \mathbf{r}} \hat{x} \right)^T$$

### Stage I-3 Curvature Discrimination (if $s \neq \text{parab}$ )

In this step the paraboloid patches are refined according to the fitted curvatures.

If  $\max(|\kappa_x|, |\kappa_y|) < \epsilon_k$  (a small threshold), set  $s = \text{plane}$ ,  $b = \text{ellipse}$ , and  $\mathbf{r}_{xy} = \mathbf{r}_{xy}(\mathbf{r})$ . Given the covariance matrix from the previous step  $\Sigma_{\mathbf{k}, \mathbf{r}, \mathbf{c}} \in \mathbb{R}^{8 \times 8}$ , we extract the new

covariance matrix  $\Sigma_{\mathbf{r}_{xy}, \mathbf{c}} \in \mathbb{R}^{5 \times 5}$  as follows:

$$\Sigma_{\mathbf{r}_{xy}, \mathbf{c}} = \mathbf{J} \Sigma_{\mathbf{k}, \mathbf{r}, \mathbf{c}} \mathbf{J}^T \in \mathbb{R}^{5 \times 5} \quad (6)$$

$$\mathbf{J} = \begin{bmatrix} \mathbf{0}_{2 \times 2} & \frac{\partial \mathbf{r}_{xy}}{\partial \mathbf{r}} & \mathbf{0}_{2 \times 3} \\ \mathbf{0}_{3 \times 2} & \mathbf{0}_{3 \times 3} & \mathbf{0}_{3 \times 3} \end{bmatrix} \in \mathbb{R}^{5 \times 8}$$

**Else if**  $\min(|\kappa_x|, |\kappa_y|) < \epsilon_k$ :

**If**  $|\kappa_y| > \epsilon_k$  set  $s = \text{cyl parab}$  and  $k = \kappa_y$ . Given the input covariance matrix  $\Sigma_{\mathbf{k}, \mathbf{r}, \mathbf{c}} \in \mathbb{R}^{8 \times 8}$  compute the *output*  $\Sigma_{\mathbf{k}, \mathbf{r}, \mathbf{c}} \in \mathbb{R}^{7 \times 7}$  as follows:

$$\Sigma_{\mathbf{k}, \mathbf{r}, \mathbf{c}} = \mathbf{J} \Sigma_{\mathbf{k}, \mathbf{r}, \mathbf{c}} \mathbf{J}^T \in \mathbb{R}^{7 \times 7} \quad (7)$$

$$\mathbf{J} = \begin{bmatrix} [0 \ 1] & \mathbf{0}_{1 \times 3} & \mathbf{0}_{1 \times 3} \\ \mathbf{0}_{3 \times 2} & \mathbf{I}_{3 \times 3} & \mathbf{0}_{3 \times 3} \\ \mathbf{0}_{3 \times 2} & \mathbf{0}_{3 \times 3} & \mathbf{I}_{3 \times 3} \end{bmatrix} \in \mathbb{R}^{7 \times 8}$$

**Else** swap axes s.t.  $|\kappa_y| > \epsilon_k$ , then set  $s = \text{cyl parab}$ ,  $k = \kappa_y$ , and  $\mathbf{r}' = \mathbf{r}(\mathbf{R}(\mathbf{r}))[\hat{\mathbf{y}} \ -\hat{\mathbf{x}} \ \hat{\mathbf{z}}]$  (log map). Given the input covariance matrix  $\Sigma_{\mathbf{k}, \mathbf{r}, \mathbf{c}} \in \mathbb{R}^{8 \times 8}$ , we compute the *output*  $\Sigma_{\mathbf{k}, \mathbf{r}, \mathbf{c}} \in \mathbb{R}^{7 \times 7}$  as follows:

$$\Sigma_{\mathbf{k}, \mathbf{r}, \mathbf{c}} = \mathbf{J} \Sigma_{\mathbf{k}, \mathbf{r}, \mathbf{c}} \mathbf{J}^T \in \mathbb{R}^{7 \times 7} \quad (8)$$

$$\mathbf{J} = \begin{bmatrix} [0 \ 1] & \mathbf{0}_{1 \times 3} & \mathbf{0}_{1 \times 3} \\ \mathbf{0}_{3 \times 2} & \frac{\partial \mathbf{r}'}{\partial \mathbf{r}} & \mathbf{0}_{3 \times 3} \\ \mathbf{0}_{3 \times 2} & \mathbf{0}_{3 \times 3} & \mathbf{I}_{3 \times 3} \end{bmatrix} \in \mathbb{R}^{7 \times 8}$$

**Else if**  $|\kappa_x - \kappa_y| < \epsilon_k$ , set  $s = \text{circ parab}$ ,  $k = \frac{\kappa_x + \kappa_y}{2}$ , and  $\mathbf{r}_{xy} = \mathbf{r}_{xy}(\mathbf{r})$ . Given the input covariance matrix  $\Sigma_{\mathbf{k}, \mathbf{r}, \mathbf{c}} \in \mathbb{R}^{8 \times 8}$  we compute the *output*  $\Sigma_{\mathbf{k}, \mathbf{r}_{xy}, \mathbf{c}} \in \mathbb{R}^{6 \times 6}$  as follows:

$$\Sigma_{\mathbf{k}, \mathbf{r}_{xy}, \mathbf{c}} = \mathbf{J} \Sigma_{\mathbf{k}, \mathbf{r}, \mathbf{c}} \mathbf{J}^T \in \mathbb{R}^{6 \times 6} \quad (9)$$

$$\mathbf{J} = \begin{bmatrix} [1/2 \ 1/2] & \mathbf{0}_{1 \times 3} & \mathbf{0}_{1 \times 3} \\ \mathbf{0}_{2 \times 2} & \frac{\partial \mathbf{r}_{xy}}{\partial \mathbf{r}} & \mathbf{0}_{2 \times 3} \\ \mathbf{0}_{3 \times 2} & \mathbf{0}_{3 \times 3} & \mathbf{I}_{3 \times 3} \end{bmatrix} \in \mathbb{R}^{6 \times 8}$$

**Else** ( $s = \text{ell parab}$ ,  $\text{hyp parab}$ ) there is no change in  $\mathbf{k}$ ,  $\mathbf{r}$ , and  $\mathbf{c}$ , and thus no change in the covariance matrix.

In this stage an unbounded patch surface fit to the data and the covariance matrix was propagated accordingly in the space of the patch parameters, depending on its type. The same process needs to be done for the boundary fitting as presented below.

**Stage II-4** Determine the Boundary Type (if  $s \neq \text{plane}$ )

In this step no action takes place, except that the type of boundary is determined. Thus, there is no change in the covariance matrix. Note that we also set  $\lambda \triangleq \sqrt{2} \text{erf}^{-1}(\Gamma)$ , which is used later during fitting.

**Stage II-5** Initialize the Bounding Parameters

In this stage the point samples are projected on the local  $xy$  patch plane and thus it is needed to propagate the uncertainty for the new projected data and their first order moments that will be used later in the fitting. Let:

$$\mathbf{m} = \begin{bmatrix} \bar{\mathbf{x}} \\ \bar{\mathbf{y}} \\ v_x \\ v_y \\ v_{xy} \end{bmatrix} = \begin{bmatrix} \hat{\mathbf{x}}^T \mathbf{X}_r(\mathbf{q}_i, \mathbf{r}, \mathbf{c}) \\ \hat{\mathbf{y}}^T \mathbf{X}_r(\mathbf{q}_i, \mathbf{r}, \mathbf{c}) \\ (\hat{\mathbf{x}}^T \mathbf{X}_r(\mathbf{q}_i, \mathbf{r}, \mathbf{c}))^2 \\ (\hat{\mathbf{y}}^T \mathbf{X}_r(\mathbf{q}_i, \mathbf{r}, \mathbf{c}))^2 \\ [(\hat{\mathbf{x}}^T \mathbf{X}_r(\mathbf{q}_i, \mathbf{r}, \mathbf{c}))(\hat{\mathbf{y}}^T \mathbf{X}_r(\mathbf{q}_i, \mathbf{r}, \mathbf{c}))] \end{bmatrix}, \quad (10)$$

where  $\bar{\mathbf{x}}$ ,  $\bar{\mathbf{y}}$  are the average projected samples,  $v_x$ ,  $v_y$ , and  $v_{xy}$  their first order moments, and  $\mathbf{q}_i' \triangleq \mathbf{X}_r(\mathbf{q}_i, \mathbf{r}, \mathbf{c}) = \mathbf{R}(-\mathbf{r})(\mathbf{q}_i - \mathbf{c}) = (\mathbf{R}(\mathbf{r}))^T(\mathbf{q}_i - \mathbf{c})$ . Then, given the covariance matrix  $\Sigma_{\mathbf{k}, \mathbf{r}, \mathbf{c}} \in \mathbb{R}^{(n_k + n_r + 3)^2}$  of the sample points and patch parameters ( $n_k$  curvatures and  $n_r$  rotation vectors, depending on the patch type), the propagated covariance matrix  $\Sigma_{\mathbf{m}, \mathbf{k}, \mathbf{r}, \mathbf{c}} \in \mathbb{R}^{(5 + n_k + n_r + 3)^2}$  is computed as follows:

$$\Sigma_{\mathbf{m}, \mathbf{k}, \mathbf{r}, \mathbf{c}} = \mathbf{J} \Sigma_{\mathbf{q}_1 \dots \mathbf{q}_N, \mathbf{k}, \mathbf{r}, \mathbf{c}} \mathbf{J}^T \in \mathbb{R}^{(5 + n_k + n_r + 3)^2} \quad (11)$$

$$\mathbf{J} = \begin{bmatrix} \frac{\partial \mathbf{m}}{\partial \mathbf{q}_1} \dots \frac{\partial \mathbf{m}}{\partial \mathbf{q}_N} & \mathbf{0}_{5 \times n_k} & \frac{\partial \mathbf{m}}{\partial \mathbf{r}} & \frac{\partial \mathbf{m}}{\partial \mathbf{c}} \\ \mathbf{0}_{n_k \times 3} \dots \mathbf{0}_{n_k \times 3} & \mathbf{I}_{n_k \times n_k} & \mathbf{0}_{n_k \times n_r} & \mathbf{0}_{n_k \times 3} \\ \mathbf{0}_{n_r \times 3} \dots \mathbf{0}_{n_r \times 3} & \mathbf{0}_{n_r \times n_k} & \mathbf{I}_{n_r \times n_r} & \mathbf{0}_{n_r \times 3} \\ \mathbf{0}_{3 \times 3} \dots \mathbf{0}_{3 \times 3} & \mathbf{0}_{3 \times n_k} & \mathbf{0}_{3 \times n_r} & \mathbf{I}_{3 \times 3} \end{bmatrix}$$

$$\mathbf{J} \in \mathbb{R}^{(5 + n_k + n_r + 3) \times (3N + n_k + n_r + 3)}$$

**Stage II-6** Cylindrical Paraboloid and Circular Cylinder

In this step the translation vector is realigned given the projected data, such that  $\mathbf{c}' = \mathbf{R}(\mathbf{r})(\bar{\mathbf{x}}\hat{\mathbf{x}}) + \mathbf{c}$  and the bound is set as  $\mathbf{d}_r = \lambda[\sqrt{v_x - \bar{\mathbf{x}}^2} \ \sqrt{v_y}]^T$ . Given the covariance matrix  $\Sigma_{\mathbf{m}, \mathbf{k}, \mathbf{r}, \mathbf{c}} \in \mathbb{R}^{12 \times 12}$ , the propagated  $\Sigma_{\mathbf{d}, \mathbf{k}, \mathbf{r}, \mathbf{c}} \in \mathbb{R}^{9 \times 9}$  one can be calculated as follows:

$$\Sigma_{\mathbf{d}, \mathbf{k}, \mathbf{r}, \mathbf{c}} = \mathbf{J} \Sigma_{\mathbf{m}, \mathbf{k}, \mathbf{r}, \mathbf{c}} \mathbf{J}^T \in \mathbb{R}^{12 \times 12} \quad (12)$$

$$\mathbf{J} = \begin{bmatrix} \frac{\partial \mathbf{d}_r}{\partial \mathbf{m}} & \mathbf{0}_{2 \times 1} & \mathbf{0}_{2 \times 3} & \mathbf{0}_{2 \times 3} \\ \mathbf{0}_{1 \times 9} & 1 & \mathbf{0}_{1 \times 3} & \mathbf{0}_{1 \times 3} \\ \mathbf{0}_{3 \times 5} & \mathbf{0}_{3 \times 1} & \mathbf{I}_{3 \times 3} & \mathbf{0}_{3 \times 3} \\ \frac{\partial \mathbf{c}'}{\partial \mathbf{m}} & \mathbf{0}_{3 \times 1} & \frac{\partial \mathbf{c}'}{\partial \mathbf{r}} & \frac{\partial \mathbf{c}'}{\partial \mathbf{c}} \end{bmatrix} \in \mathbb{R}^{9 \times 12}$$

**Stage II-7** Circular Paraboloid and Sphere

In this step the bound is set as  $\mathbf{d}_c = \lambda \max(\sqrt{v_x}, \sqrt{v_y})$ . Given the covariance matrix  $\Sigma_{\mathbf{m}, \mathbf{k}, \mathbf{r}_{xy}, \mathbf{c}} \in \mathbb{R}^{11 \times 11}$ , the propagated  $\Sigma_{\mathbf{d}_c, \mathbf{k}, \mathbf{r}_{xy}, \mathbf{c}} \in \mathbb{R}^{9 \times 9}$  one can be calculated as follows:

$$\Sigma_{\mathbf{d}_c, \mathbf{k}, \mathbf{r}_{xy}, \mathbf{c}} = \mathbf{J} \Sigma_{\mathbf{m}, \mathbf{k}, \mathbf{r}_{xy}, \mathbf{c}} \mathbf{J}^T \in \mathbb{R}^{11 \times 11} \quad (13)$$

$$\mathbf{J} = \begin{bmatrix} \frac{\partial \mathbf{d}_c}{\partial \mathbf{m}} & 0 & \mathbf{0}_{1 \times 2} & \mathbf{0}_{1 \times 3} \\ \mathbf{0}_{1 \times 5} & 1 & \mathbf{0}_{1 \times 2} & \mathbf{0}_{1 \times 3} \\ \mathbf{0}_{2 \times 5} & \mathbf{0}_{2 \times 1} & \mathbf{I}_{2 \times 2} & \mathbf{0}_{2 \times 3} \\ \mathbf{0}_{3 \times 5} & \mathbf{0}_{3 \times 1} & \mathbf{0}_{3 \times 2} & \mathbf{I}_{3 \times 3} \end{bmatrix} \in \mathbb{R}^{7 \times 11}$$

**Stage II-8** Elliptic and Hyperbolic Paraboloid

In this step the bound is set as  $\mathbf{d}_e = \lambda[\sqrt{v_x} \ \sqrt{v_y}]^T$ . Given the covariance matrix  $\Sigma_{\mathbf{m}, \mathbf{k}, \mathbf{r}, \mathbf{c}} \in \mathbb{R}^{11 \times 11}$ , the propagated  $\Sigma_{\mathbf{d}_e, \mathbf{k}, \mathbf{r}, \mathbf{c}} \in \mathbb{R}^{13 \times 13}$  one can be calculated as follows:

$$\Sigma_{\mathbf{d}_e, \mathbf{k}, \mathbf{r}, \mathbf{c}} = \mathbf{J} \Sigma_{\mathbf{m}, \mathbf{k}, \mathbf{r}, \mathbf{c}} \mathbf{J}^T \in \mathbb{R}^{13 \times 13} \quad (14)$$

$$\mathbf{J} = \begin{bmatrix} \frac{\partial \mathbf{d}_e}{\partial \mathbf{m}} & \mathbf{0}_{2 \times 2} & \mathbf{0}_{2 \times 3} & \mathbf{0}_{2 \times 3} \\ \mathbf{0}_{2 \times 5} & \mathbf{I}_{2 \times 2} & \mathbf{0}_{2 \times 3} & \mathbf{0}_{2 \times 3} \\ \mathbf{0}_{3 \times 5} & \mathbf{0}_{3 \times 2} & \mathbf{I}_{3 \times 3} & \mathbf{0}_{3 \times 3} \\ \mathbf{0}_{3 \times 5} & \mathbf{0}_{3 \times 2} & \mathbf{0}_{3 \times 3} & \mathbf{I}_{3 \times 3} \end{bmatrix} \in \mathbb{R}^{13 \times 10}$$

**Stage II-9** Plane

This is the most tedious step case, given the four different options of planar bounds. The vectors  $\mathbf{r}_{xy}$  and  $\mathbf{c}$  are available either from Stage I-1 or I-3. We set  $\mathbf{c}' = \mathbf{X}_f(\bar{\mathbf{x}}\hat{\mathbf{x}} + \bar{\mathbf{y}}\hat{\mathbf{y}}, \mathbf{r}_{xy}, \mathbf{c}) = \mathbf{R}\left(\begin{bmatrix} \mathbf{r}_{xy} \\ 0 \end{bmatrix}\right)(\bar{\mathbf{x}}\hat{\mathbf{x}} + \bar{\mathbf{y}}\hat{\mathbf{y}}) + \mathbf{c}$  and following [20], we

let:

$$\rho \triangleq [\alpha \ \beta \ \phi]^T = [v_x - \bar{x}^2 \ 2v_{xy} - \bar{x}\bar{y} \ v_y - \bar{y}^2]^T$$

$$\mathbf{l} \triangleq \begin{bmatrix} l_+ \\ l_- \end{bmatrix} = \sqrt{-\ln(1-\Gamma)} \begin{bmatrix} \sqrt{\alpha + \phi + \sqrt{D}} \\ \sqrt{\alpha + \phi - \sqrt{D}} \end{bmatrix}$$

$$D \triangleq \beta^2 + (\alpha - \phi)^2$$

Given the covariance matrix  $\Sigma_{\mathbf{m},\mathbf{k},\mathbf{r}_{xy},\mathbf{c}} \in \mathbb{R}^{10 \times 10}$ , the propagated  $\Sigma_{\mathbf{l},\rho,\mathbf{r}_{xy},\mathbf{c}'} \in \mathbb{R}^{10 \times 10}$  matrix can be calculated as follows:

$$\Sigma_{\mathbf{l},\rho,\mathbf{r}_{xy},\mathbf{c}'} = \mathbf{J} \Sigma_{\mathbf{m},\mathbf{k},\mathbf{r}_{xy},\mathbf{c}} \mathbf{J}^T \in \mathbb{R}^{10 \times 10} \quad (15)$$

$$\mathbf{J} = \begin{bmatrix} \frac{\partial \mathbf{l}}{\partial \mathbf{m}} & \mathbf{0}_{2 \times 2} & \mathbf{0}_{2 \times 3} \\ \frac{\partial \rho}{\partial \mathbf{m}} & \mathbf{0}_{3 \times 2} & \mathbf{0}_{3 \times 3} \\ \mathbf{0}_{2 \times 5} & \mathbf{I}_{2 \times 2} & \mathbf{0}_{2 \times 3} \\ \frac{\partial \mathbf{c}'}{\partial \mathbf{m}} & \frac{\partial \mathbf{c}'}{\partial \mathbf{r}_{xy}} & \frac{\partial \mathbf{c}'}{\partial \mathbf{c}} \end{bmatrix} \in \mathbb{R}^{13 \times 10}$$

If  $\mathbf{b}=\text{circle}$ , the bound is set as  $d_c = \max(l_+, l_-)$  and the propagated  $\Sigma_{d_c,\mathbf{r}_{xy},\mathbf{c}'} \in \mathbb{R}^{6 \times 6}$  covariance can be calculated as follows:

$$\Sigma_{d_c,\mathbf{r}_{xy},\mathbf{c}'} = \mathbf{J} \Sigma_{\mathbf{l},\rho,\mathbf{r}_{xy},\mathbf{c}'} \mathbf{J}^T \in \mathbb{R}^{6 \times 6} \quad (16)$$

$$\mathbf{J} = \begin{bmatrix} \frac{\partial d_c}{\partial \mathbf{l}} & \mathbf{0}_{1 \times 3} & \mathbf{0}_{1 \times 2} & \mathbf{0}_{1 \times 3} \\ \mathbf{0}_{2 \times 2} & \mathbf{0}_{2 \times 3} & \mathbf{I}_{2 \times 2} & \mathbf{0}_{2 \times 3} \\ \mathbf{0}_{3 \times 2} & \mathbf{0}_{3 \times 3} & \mathbf{0}_{3 \times 2} & \mathbf{I}_{3 \times 3} \end{bmatrix} \in \mathbb{R}^{6 \times 10}$$

Similarly if  $\mathbf{b} \in \{\text{ellipse}, \text{arect}, \text{conv quad}\}$ , with a boundary vector  $\mathbf{d}$ , the propagated  $\Sigma_{\mathbf{d},\mathbf{r},\mathbf{c}'} \in \mathbb{R}^{(n_d+6) \times (n_d+6)}$  covariance matrix can be calculated as follows:

$$\Sigma_{\mathbf{d},\mathbf{r},\mathbf{c}'} = \mathbf{J} \Sigma_{\mathbf{l},\rho,\mathbf{r}_{xy},\mathbf{c}'} \mathbf{J}^T \in \mathbb{R}^{(n_d+6) \times (n_d+6)} \quad (17)$$

$$\mathbf{J} = \begin{bmatrix} \frac{\partial \mathbf{d}}{\partial \mathbf{l}} & \mathbf{0}_{n_d \times 3} & \mathbf{0}_{n_d \times 2} & \mathbf{0}_{n_d \times 3} \\ \mathbf{0}_{3 \times 2} & \frac{\partial \mathbf{r}}{\partial \rho} & \frac{\partial \mathbf{r}}{\partial \mathbf{r}_{xy}} & \mathbf{0}_{3 \times 3} \\ \mathbf{0}_{3 \times 2} & \mathbf{0}_{3 \times 3} & \mathbf{0}_{3 \times 2} & \mathbf{I}_{3 \times 3} \end{bmatrix} \in \mathbb{R}^{(n_d+6) \times 10}$$

This concludes the first order error propagation from the point samples to the patch parameters for all the ten patch types. More details can be found in the implementation of the propagation in [21]. We now present the uncertainty evaluation metrics for the propagated covariances and some experimental results.

#### IV. UNCERTAINTY METRICS

To quantitatively evaluate the magnitude of the propagated Gaussian uncertainty, we define a set of distance metrics. Given that the propagated covariance matrix is in the space of the geometrically meaningful patch parameters, i.e. rotation, translation, and boundary sizes/angles, the introduced metrics are defined in each of these spaces. Using these metrics, we run validation experiments on point cloud data that are generated by simulated or real range sensors. In the former case we use the data ground truth for evaluation, whereas in the latter one we analyze the metrics on data from a real curved rocky surface. These metrics provide quantitative uncertainty measures that can be further used for risk contact planning analysis.

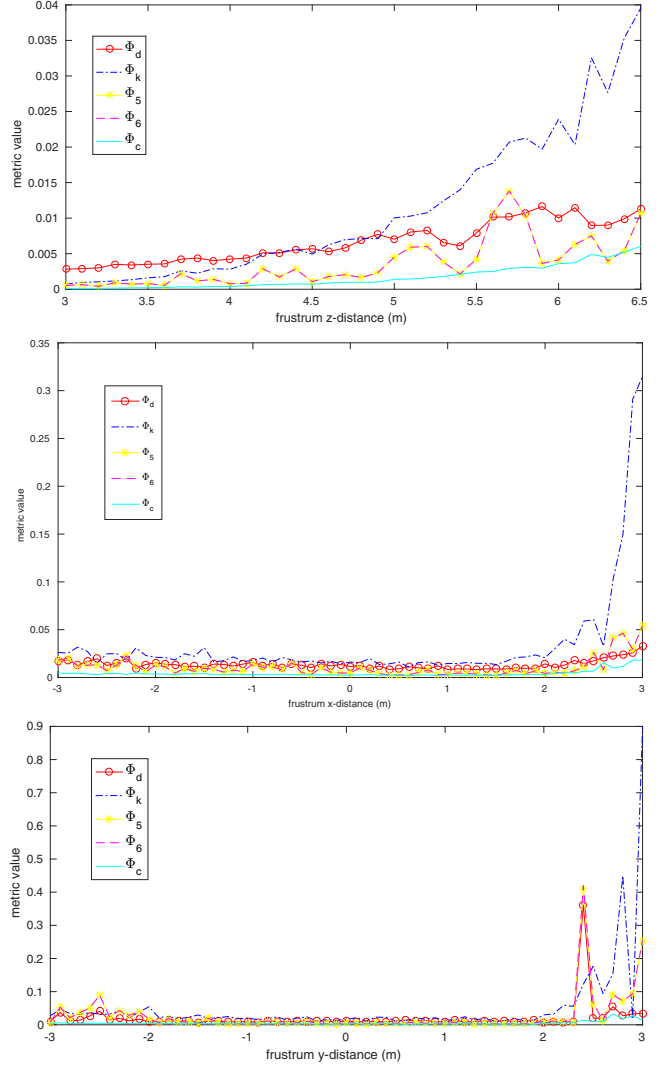


Fig. 5. All the uncertainty metrics (y-axis) for an elliptic paraboloid, from different frustum x, y, and z positions (x-axis).

#### A. Multivariate Gaussian Distribution Metrics

To analyze the uncertainty after the patch fitting and the uncertainty propagation, we use the estimated vector of parameters and the propagated covariance matrix. Assuming multivariate normal (Gaussian) distribution that follows the propagated patch covariance, we randomly sample a set  $n_v$  of parameter vectors, each one representing a *sampled patch*. In this way we can analyze the distribution of every (set of) parameter(s) under the propagated uncertainty.

We first evaluate the rotation uncertainty, based on two distance metrics that were introduced in [22]. The *Deviation from the Identity Matrix* ( $\Phi_5$ ) metric is defined as follows. Given the rotation matrix  $\mathbf{R}_p \in SO(3)$  of the fitted patch and the corresponding  $\mathbf{R}_s \in SO(3)$  for the sampled patch:

$$\Phi_5(\mathbf{R}_p, \mathbf{R}_s) = \|\mathbf{I} - \mathbf{R}_p \mathbf{R}_s^T\|_2 \quad (18)$$

$$\Phi_5 : SO(3) \times SO(3) \rightarrow \mathbb{R}^+ \in [0, 2].$$

This metric is a distance measure of the angle between two rigid body displacements and takes values between 0 and 2. It is equivalent to:  $\cos^{-1}(((\text{trace}(\mathbf{R}_p^T \mathbf{R}_s) - 1)/2))$ . Similarly

surface	bound	parameters		DoF	$\Phi_d$ (m)	$\Phi_k$ (m <sup>-1</sup> )	$\Phi_5$ (rad)	$\Phi_6$ (rad)	$\Phi_t$ (m)
		intrin.	extrin.		$\mu \pm \sigma$	$\mu \pm \sigma$	$\mu \pm \sigma$	$\mu \pm \sigma$	$\mu \pm \sigma$
ell parab	ellipse	$\mathbf{d}_e, \mathbf{k}$	$\mathbf{r}, \mathbf{c}$	10	$0.012 \pm (4 \cdot 10^{-5})$	$0.019 \pm (1 \cdot 10^{-4})$	$0.005 \pm (1 \cdot 10^{-5})$	$0.005 \pm (1 \cdot 10^{-5})$	$0.003 \pm (5 \cdot 10^{-6})$
hyp parab	ellipse	$\mathbf{d}_e, \mathbf{k}$	$\mathbf{r}, \mathbf{c}$	10	$0.008 \pm (2 \cdot 10^{-5})$	$0.016 \pm (1 \cdot 10^{-4})$	$0.001 \pm (3 \cdot 10^{-7})$	$0.001 \pm (3 \cdot 10^{-7})$	$0.002 \pm (4 \cdot 10^{-6})$
cyl parab	aa rect	$\mathbf{d}_r, \kappa$	$\mathbf{r}, \mathbf{c}$	9	$0.008 \pm (3 \cdot 10^{-5})$	$0.031 \pm (5 \cdot 10^{-4})$	$0.001 \pm (3 \cdot 10^{-7})$	$0.001 \pm (3 \cdot 10^{-7})$	$0.004 \pm (5 \cdot 10^{-6})$
circ parab	circle	$\mathbf{d}_c, \kappa$	$\mathbf{r}_{xy}, \mathbf{c}$	7	$0.010 \pm (3 \cdot 10^{-5})$	$0.002 \pm (2 \cdot 10^{-6})$	$0.018 \pm (2 \cdot 10^{-4})$	$0.018 \pm (2 \cdot 10^{-4})$	$(8821 \pm 4) \cdot 10^{-7}$
plane	ellipse	$\mathbf{d}_e$	$\mathbf{r}, \mathbf{c}$	8	$0.008 \pm (2 \cdot 10^{-5})$	—	$0.003 \pm (5 \cdot 10^{-8})$	$0.003 \pm (5 \cdot 10^{-8})$	$0.002 \pm (2 \cdot 10^{-6})$
	circle	$\mathbf{d}_c$	$\mathbf{r}_{xy}, \mathbf{c}$	6	$0.008 \pm (2 \cdot 10^{-5})$	—	$0.002 \pm (2 \cdot 10^{-6})$	$0.002 \pm (2 \cdot 10^{-6})$	$0.002 \pm (1 \cdot 10^{-3})$
	aa rect	$\mathbf{d}_r$	$\mathbf{r}, \mathbf{c}$	8	$0.007 \pm (1 \cdot 10^{-5})$	—	$0.002 \pm (3 \cdot 10^{-6})$	$0.002 \pm (3 \cdot 10^{-6})$	$0.003 \pm (1 \cdot 10^{-6})$
	c quad	$\mathbf{d}_q$	$\mathbf{r}, \mathbf{c}$	11	$0.010 \pm (3 \cdot 10^{-5})$	—	$0.004 \pm (8 \cdot 10^{-6})$	$0.004 \pm (8 \cdot 10^{-6})$	$(20 \pm 3) \cdot 10^{-6}$
sphere	circle	$\mathbf{d}_c, \kappa$	$\mathbf{r}_{xy}, \mathbf{c}$	7	$0.005 \pm (1 \cdot 10^{-5})$	$2 \cdot 10^{-8} \pm (1 \cdot 10^{-12})$	$0.025 \pm (3 \cdot 10^{-4})$	$0.025 \pm (3 \cdot 10^{-4})$	$0 \pm (2 \cdot 10^{-12})$
circ cylind	aa rect	$\mathbf{d}_r, \kappa$	$\mathbf{r}, \mathbf{c}$	9	$0.006 \pm (1 \cdot 10^{-5})$	$3 \cdot 10^{-6} \pm (6 \cdot 10^{-12})$	$7.59 \cdot 10^{-9} \pm 10^{-12}$	$7.59 \cdot 10^{-9} \pm 10^{-12}$	$0.002 \pm (2 \cdot 10^{-6})$

TABLE I

the *Geodesic on the Unit Sphere* ( $\Phi_6$ ) metric is defined as:

$$\Phi_6(\mathbf{R}_p, \mathbf{R}_s) = \|\log(\mathbf{R}_p \mathbf{R}_s^T)\| \quad (19)$$

$$\Phi_6 : SO(3) \times SO(3) \rightarrow \mathbb{R}^+ \in [0, \pi].$$

This metric that takes values between 0 and  $\pi$  is an alternative form to evaluate the magnitude of the rotation angle. Note that the relation of these two metrics is defined as  $\Phi_5 = 2\sin(\Phi_6/2)$  and thus, we notice that for small rotation values their numerical difference is negligible.

To evaluate the translation (i.e. patch central point), we just use the *Euclidean Distance*, i.e. norm, ( $\Phi_t \in \mathbb{R}$ ) between the fitted  $\mathbf{c}_p$  and the sampled  $\mathbf{c}_s$  such that:

$$\Phi_t = \sqrt{\mathbf{c}_p \mathbf{c}_s^T}. \quad (20)$$

For the curvatures ( $\Phi_k$  metric) and the boundary ( $\Phi_d$  metric) parameters we perform the same analysis, by calculating the norm between the fitted and the sampled parameter vectors of the curvatures and boundaries respectively.

We evaluate the introduced metrics for every sampled patch and we report their mean and variance, which gives the uncertainty estimation of each set of parameters. An other approach for evaluation could be based on the eigendecomposition of the covariance matrix, as it was presented in [5]. However, the eigenvalues/eigenvectors metrics are usually used to compare the results between different methods, which is not the case in this paper.

### B. Experimental Results

surface (bound)	parameters ( $\mathbf{k}, \mathbf{d}$ )
ell parab (ellipse)	$\mathbf{k} = [-1 \ -2]; \mathbf{d} = [1.5 \ 1]$
hyp parab (ellipse)	$\mathbf{k} = [0.5 \ -1]; \mathbf{d} = [1.5 \ 1]$
cyl parab (aa rect)	$\mathbf{k} = -2; \mathbf{d} = [2 \ 0.8]$
circ parab (circle)	$\mathbf{k} = -1; \mathbf{d} = 1.8$
plane (ellipse)	$\mathbf{d} = [1.5 \ 1]$
plane (circle)	$\mathbf{d} = 2$
plane (aa rect)	$\mathbf{d} = [1.7 \ 2.5]$
plane (c quad)	$\mathbf{d} = [2.3 \ 2 \ 1.7 \ 2.3 \ \pi/4]$
sphere (circle)	$\mathbf{k} = -1/2; \mathbf{d} = 1.8$
circ cylind (aa rect)	$\mathbf{k} = -1/2; \mathbf{d} = [2 \ 1.8]$

TABLE II

Having defined the metrics above, we run three experiments on simulated and real range data. To acquire simulated data we define manually ten patches of all different types and we sample a set of equally distributed points on their surfaces from a particular frustum. In particular, we set the frustum to point at the center of each patch in distance (-1,-1,6). The

patches are aligned with the world axes, while their center is at the world origin. Their ground truth intrinsic parameters are described in Table II (rotation and translation is implied given their position in the world frame). For each patch, we sample a set of 3D points and we perturb them using Gaussian noise that follows the covariance matrix that is specified with the process that was presented in the previous section.

In the first experiment, we run the fitting process on simulated sample points for each patch type of Table II, propagating at the same time the uncertainty. Using the output covariance matrix, we sample  $n_v=10^4$  set of patches, assuming multivariate normal distribution. In Table I we report the distance metric results (mean and variance over all the patch samples) for all the patch types. We notice that for the boundary parameters ( $\Phi_d$ ) all the patches have the same range of uncertainty, i.e. between 5 – 12mm, while the variance is negligible (in the order of  $10^{-5}$ ). More variation in the range of the results exists for the curvature metric ( $\Phi_k$ ). While we see that elliptic, hyperbolic, and cylindrical paraboloids (2 principle curvatures) appear to have an average uncertainty of  $22(\text{m}^{-1})$ , the circular paraboloid (1 curvature) has smaller uncertainty by one order of magnitude, while the sphere and circular cylinder (1 curvature) have negligible uncertainty. Moving to the extrinsic parameters, we notice that the uncertainty of the rotation angle ( $\Phi_{5,6}$ ) is of the same order for most of the patches, except the circular paraboloid (one order higher) and the circular cylinder, which is almost zero. From the other side, the uncertainty in the position ( $\Phi_t$ ) is in the order of  $10^{-3}$  for all the patches, except for the circular paraboloid and the sphere that are almost zero. All these results, which are an experimental analysis of the propagated patch uncertainty, can be used to weigh our confidence towards some patch types over others. For instance, it seems better to pick a spherical patch contact than a circular paraboloid one, since it appears to be more certain.

In the second experiment, we run the same process as above for the elliptic paraboloid, by tweaking the position of the frustum. We let its z distance from the patch to move between 3m and 6.5m and its x and y distance between -3m and 3m each, while we let the frustum always point to the center of the patch. We report the results of the metrics in Fig. 5. In the first plot, we can see that when the frustum moves away from the patch the values of the metrics are

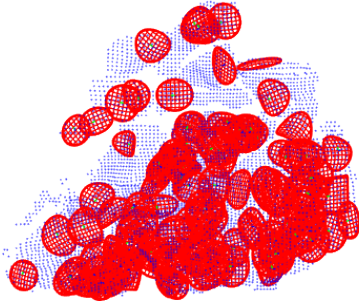


Fig. 6. 150 patches fitted to real range samples from a rocky environment.

increasing, which is very reasonable since the sample points have a bigger uncertainty in the measurement rays direction and this propagates accordingly to the patch parameters. More interestingly, it appears that the uncertainty in the curvature increases more radically than the others, while the smallest is always the boundary uncertainty. Similarly, when the angle between the frustum and the patch is changing the uncertainty appears to be stable, until an extreme is reached, where the patch is sampled from the side. Then the uncertainty increases and a lot of spikes appear in the metrics. This is also reasonable given that from the side we lose most of the geometric properties of a patch.

Last but not least, we run the same experiments for a real rock at 1.2m away from a Kinect range sensor. We fit 150 patches and we report the metric results in Fig. 6. We verify the fact that the biggest uncertainty appears in the curvature ( $\Phi_k$ ), while the rest and especially the uncertainty of the position ( $\Phi_t$ ) and boundary ( $\Phi_d$ ) are much smaller. Note that since the environment is continuous and the patches are closer to the sensor than those studied in simulation, we have smaller uncertainty values than in Table II.

## V. CONCLUSIONS AND FUTURE WORKS

In this paper we introduce a Gaussian modeling of uncertainty for bounded curved patches that fit to noisy range data. Moreover, we describe in detail the uncertainty propagation from the point samples to the fitted patch parameters, expressed as a covariance matrix. We evaluate the magnitude of uncertainty through a set of metrics in simulated and real data. The curved contact patches have been already used for locomotion and manipulation purposes on three different humanoid robots, i.e. the WALK-MAN [17], the COMAN [18], and the RBPB [16]. We are in the process of integrating the patch uncertainty propagation into our affordance interface [23], for a contact risk analysis between these robots and the environment. Moreover, we plan for an extensive uncertainty evaluation on real data, while ground truth sample points can be extracted from more accurate sensors. We also envision the patch uncertainty propagation to lead us to a patch-based SLAM system similar to [2] and a Kalman-based patch fusion, using both exteroception and proprioception, to improve the uncertainty of the contact patches over time.

## ACKNOWLEDGMENT

This work is supported by the European Union Seventh Framework Programme FP7-ICT-2013-10 under grant agreement no 611832 (WALK-MAN). Kanoulas and Vona were at Northeastern University in Boston, MA when the bulk of this work was performed with support from the National Science Foundation under Grant No. 1149235.

## REFERENCES

- [1] M. Vona and D. Kanoulas, "Curved Surface Contact Patches With Quantified Uncertainty," in *IEEE/RSJ IROS*, 2011, pp. 1439–1446.
- [2] J. Weingarten and R. Siegwart, "3D SLAM using Planar Segments," in *IEEE/RSJ IROS*, 2006, pp. 3062–3067.
- [3] D. Kanoulas and M. Vona, "Sparse Surface Modeling with Curved Patches," in *IEEE ICRA*, 2013, pp. 4209–4215.
- [4] K. Pathak, N. Vaskevicius, and A. Birk, "Revisiting Uncertainty Analysis for Optimum Planes Extracted from 3D Range Sensor Point-clouds," in *IEEE ICRA*, 2009, pp. 2035–2040.
- [5] —, "Uncertainty Analysis for Optimum Plane Extraction from Noisy 3D Range-Sensor Point-Clouds," *Intelligent Service Robotics (ISR)*, vol. 3, no. 1, pp. 37–48, 2009.
- [6] M. F. Fallon, P. Marion, R. Deits, T. Whelan, M. Antone, J. McDonald, and R. Tedrake, "Continuous Humanoid Locomotion over Uneven Terrain using Stereo Fusion," in *15th IEEE-RAS Humanoids*, 2015, pp. 881–888.
- [7] A. ten Pas and R. Platt, "Localizing Grasp Affordances in 3-D Points Clouds Using Taubin Quadric Fitting," in *ISER*, 2014, pp. 623–638.
- [8] M. T. Mason, "Creation Myths: The Beginnings of Robotics Research," *IEEE Robotics & Automation Magazine (RAM)*, vol. 19, no. 2, pp. 72–77, 2012.
- [9] L. Matthies and S. A. Shafer, "Error Modeling in Stereo Navigation," *IEEE Journal of Robotics and Automation (JRA)*, vol. RA-3, no. 3, pp. 239–250, Jun 1987.
- [10] R. B. Rusu, A. Holzbach, R. Diankov, G. Bradski, and M. Beetz, "Perception for Mobile Manipulation and Grasping using Active Stereo," in *9th IEEE-RAS Humanoids*, 2009, pp. 632–638.
- [11] M. W. Maimone, P. C. Leger, and J. J. Biesiadecki, "Overview of the Mars Exploration Rovers Autonomous Mobility and Vision Capabilities," in *IEEE ICRA*, 2007.
- [12] D. Murray and J. J. Little, "Patchlets: Representing Stereo Vision Data with Surface Elements," in *7th IEEE Workshops on Application of Computer Vision (WACV/MOTION)*, vol. 1, 2005, pp. 192–199.
- [13] K. Khoshelham and S. O. Elberink, "Accuracy and Resolution of Kinect Depth Data for Indoor Mapping Applications," in *Sensors*, vol. 12, 2012, pp. 1437–1454.
- [14] I. Dryanovski, R. G. Valentii, and J. Xiao, "Fast Visual Odometry and Mapping from RGB-D Data," in *IEEE ICRA*, 2013, pp. 2305–2310.
- [15] P. Fankhauser, M. Bloesch, C. Gehring, M. Hutter, and R. Siegwart, "Robot-Centric Elevation Mapping with Uncertainty Estimates," in *CLAWAR*, no. EPFL-CONF-198746, 2014.
- [16] D. Kanoulas, "Curved Surface Patches for Rough Terrain Perception," Ph.D. dissertation, CCIS, Northeastern University, August 2014.
- [17] N. G. Tsagarakis *et al.*, "WALK-MAN: A High Performance Humanoid Platform for Realistic Environments," *Journal of Field Robotics (JFR)*, 2016.
- [18] D. Kanoulas, J. Lee, D. G. Caldwell, and N. G. Tsagarakis, "Visual Grasp Affordance Localization in Point Clouds using Curved Contact Patches," *International Journal of Humanoid Robotics (IJHR)*, 2016.
- [19] S. L. Meyer, *Data Analysis for Scientists and Engineers*. Peer Management Consultants, Ltd., 1992.
- [20] L. Rocha, L. Velho, and P. C. P. Carvalho, "Image Moments-based Structuring and Tracking of Objects," in *Brazilian Symposium on Computer Graphics and Image Processing*, 2002, pp. 99–105.
- [21] D. Kanoulas and M. Vona, "The Surface Patch Library (SPL)," in *IEEE ICRA Workshop: MATLAB/Simulink for Robotics Education and Research*, 2014, <http://dkanou.github.io/projects/spl/index.html>.
- [22] D. Q. Huynh, "Metrics for 3D Rotations: Comparison and Analysis," *J. Math. Imaging Vis.*, vol. 35, no. 2, pp. 155–164, Oct 2009.
- [23] P. Kaiser, D. Kanoulas, M. Grotz, L. Muratore, A. Rocchi, E. M. Hoffman, N. G. Tsagarakis, and T. Asfour, "An Affordance-Based Pilot Interface for High-Level Control of Humanoid Robots in Supervised Autonomy," in *16th IEEE-RAS Humanoids*, 2016.